Report
P-20-01
March 2020

Modelling matrix diffusion in Task 9B – LTDE-SD

Task 9 of SKB Task Force GWFTS – Increasing the realism in solute transport modelling based on the field experiments REPRO and LTDE-SD

Shuo Meng
Luis Moreno
Ivars Neretnieks
Longcheng Liu

SVENSK KÄRNBRÄNSLEHANTERING AB

SWEDISH NUCLEAR FUEL
AND WASTE MANAGEMENT CO

Box 3091, SE-169 03 Solna
Phone +46 8 459 84 00
skb.se

SVENSK KÄRNBRÄNSLEHANTERING

ISSN 1651-4416
SKB P-20-01
ID 1890453
March 2020

Modelling matrix diffusion in Task 9B – LTDE-SD

Task 9 of SKB Task Force GWFTS – Increasing the realism in solute transport modelling based on the field experiments REPRO and LTDE-SD

Shuo Meng, Luis Moreno, Ivars Neretnieks, Longcheng Liu
Royal Institute of Technology, KTH

Keywords: In situ tracer test, Inverse modelling, Predictive modelling, Diffusion, Sorption.

Abstract

Task 9B concerns modelling of the field experiment LTDE-SD within SKB Task Force GWFTS, which was carried out in Äspö Hard Rock Laboratory, at about 410 m depth. Task description and accompanying data are found in Löfgren and Nilsson (2020). The Task comprises inverse and predictive modelling of concentration profiles within the rock. For the simulations, a conventional matrix diffusion and sorption model was applied. A mass balance was also done, which shows the non-identified losses were significant for some tracers, in particular for the strongly sorbing ones, where the non-identified fraction was around 50 %. Effective diffusion coefficients were determined. The effective diffusion coefficients for Na-22 were similar to those from the literature, while the values for Ba-133 were slightly higher and the values for Cs-137 were higher. The higher values for Cs are possibly due to surface diffusion. Cl-36 shows a very low effective diffusion coefficient caused probably by anion exclusion.

Sammanfattning

Uppgift 9B avser modelleringen av fältförsöket LTDE-SD inom SKB Task Force GWFTS. Fältförsöket genomfördes i Äspö Hard Rock Laboratory, på cirka 410 m djup. Uppgiftsbeskrivning och tillhörande data återfinns i Löfgren och Nilsson (2020). Uppgiften innefattar den inversa och prediktiva modelleringen av penetrationsprofilerna. För simuleringarna användes en konventionell matrisdiffusions- och sorptionsmodell. En massbalans gjordes också, vilken påvisar att de icke-identifierade förlusterna var betydande för vissa spårämnen, särskilt för de starkt sorberande, där denna fraktion var cirka 50 %. Effektiva diffusionskoefficienter bestämdes. Vad det gäller de effektiva diffusionskoefficienterna, så är de för Na-22 enligt de från litteraturen, för Ba-133 är de något högre och för Cs-137 högre. Det högre värdena för Cs kan bero på ytdiffusion. Cl-36 uppvisar mycket låga värden förmodligen orsakade av anjonsuteslutning.

Contents

1 Introduction

We have modelled the LTDE-SD experiments following the guidelines found in the Task 9B Descriptions (Löfgren and Nilsson 2020). The original Task Description included several tasks: Tasks 9B-1, 9B-2 and 9B-3. However, the present report has a different structure, since the most of the experimental data is known, at present. Therefore, the report includes firstly predictive modelling using parameters from literature and where the results are compared with the experimental data. In the second part, the experimental concentration profiles are fitted. The fitted parameters are the effective diffusion coefficient and the capacity factor, which is defined as ($\alpha_p = (\varepsilon + K_{dp})$).

1.1 Background

We have worked with flow and transport in fractured crystalline rocks with porous matrices a long time. Our interest is primarily aimed at applications to nuclear waste repositories. We have over the years developed analytical and numerical computation tools suitable for such applications and have performed numerous field and laboratory experiments related to this problem.

Task 9 is part of the SKB Task Force on Modelling of Groundwater Flow and Transport of Solutes (Task Force GWFTS). It focuses on the realistic modelling of coupled matrix diffusion and sorption in the heterogeneous crystalline rock matrix at depth. Task 9B focuses on the inverse and predictive modelling of experimental results from the in situ tracer test LTDE-SD (Long Term Sorption Diffusion Experiment), which was carried out using radioactive tracers at a depth of about 410 m below sea level within the Äspö Hard Rock Laboratory in Sweden.

In Task 9B, all tracers diffuse into the fracture coating and rock matrix surrounding the experimental sections of the LTDE-SD borehole during the ~200 days of exposure to the tracer cocktail. After experiments, rock samples surrounding the injection hole were drilled, and tracer content were measured and analysed. A-core samples were drilled from the exposed fracture surface while D-core samples were drilled from the rock around the slim hole, as shown in Figure 1-1 (Löfgren and Nilsson 2020).

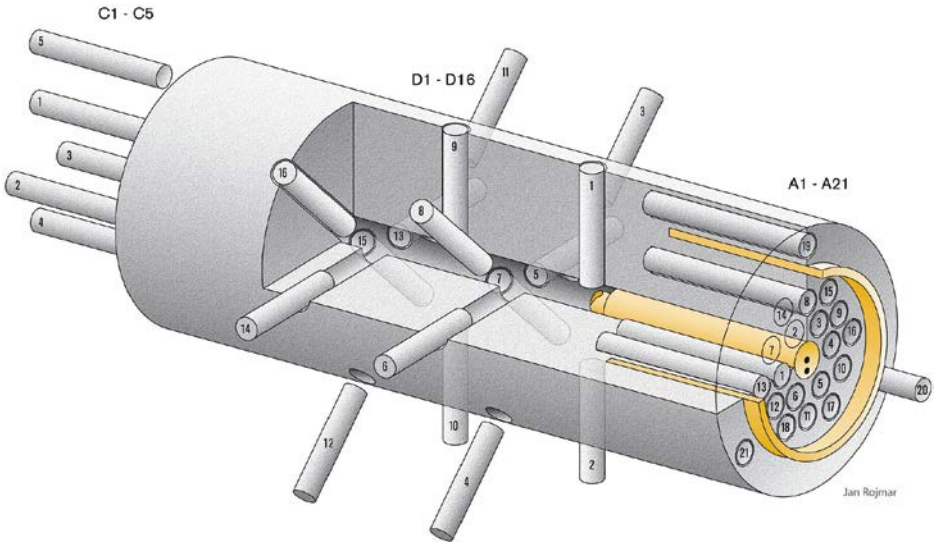

Figure 1-1. *Layout of the experiment (Nilsson et al. 2010).*

It should be noted that most core samples were sawn into cuboids prior to the slicing, hence removing the outer cylindrical mantel that could have been subjected to contamination during the core drilling. Drilled samples were then cut into slices for facilitating following analysis of their radionuclide content. The first three slices closest to the tracer cocktail/rock interfaces were sawn into a thickness of ~1 mm. The next three slices were sawn with a thickness of ~3 mm; the following three slices were ~5 mm thick; the following three slices were ~10 mm thick; and the last three slices had a thickness of 20 mm. A loss of about 0.3 mm between each slice can be considered (Löfgren and Nilsson 2020). A partition diagram of a typical sawing of a core sample is shown in Figure 1-2 (Nilsson et al. 2010).

The tracer cocktail contained the 22 radionuclides Na-22, S-35, Cl-36, Co-57, Ni-63, Se-75, Sr-85, Nb-95, Zr-95, Tc-99, Pd-102, Cd 109, Ag-110, Sn-113, Ba-133, Cs-137, Gd-153, Hf-175, Ra-226, Pa-233, U-236, and Np-237. The performances of 11 tracers in rock cores will be analysed.

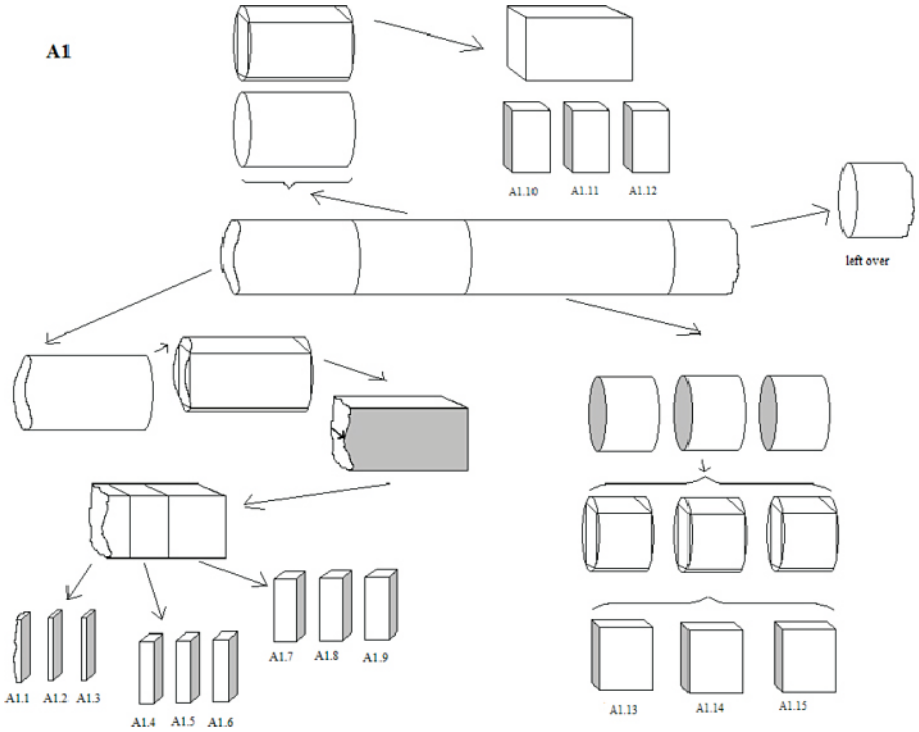

Figure 1-2. *Illustration of the sampling of the A1-core from the over-cored rock volume in LTDE-SD. Reproduced from Nilsson et al. (2010, Figure 2-10).*

1.2 Objectives

The first objective of LTDE-SD was to investigate the magnitude and extent of diffusion into matrix rock from a natural fracture in situ under natural rock stress conditions and hydraulic pressure and groundwater chemical conditions. In addition, data on sorption properties on natural fracture surfaces and internal surfaces in the matrix will be obtained. Those estimated data will be compared with laboratory derived diffusion constants and sorption coefficients for the investigated rock fracture system, for the purpose of evaluating whether laboratory scale sorption results are representative also for large scales (Löfgren and Nilsson 2020).

The objective of the Task 9B was to familiarise ourselves with the LTDE-SD experiments and to do some inverse modelling of the activity profiles of the tracers in the cores (9B-1 and 9B-2). We also applied established models to predict the tracer distribution profile (9B-3).

In Task 9B-1, we would perform inverse modelling for six tracers (Na-22, Cl-36, Co-57, Ni-63, Ba-133 and Cs-137) in four different cores (A6, A9, D12 and D13). A central case should be provided where the profiles are reproduced with justifiable input data. In Task 9B-2, inverse modelling would be performed not only for the mentioned six tracers but also for five new tracers, i.e. Cd-109, Ag-110, Gd-153, Ra-226 and Np-237. Their performances in all A- and D-cores (A1, A5, A6, A8, A9, A10, A12, A15, A16, A17, A20, D1, D5, D6, D7, D8, D12, D13 and D14) (Löfgren and Nilsson 2020).

By contrast, the idea of Task 9B-3 is to use the models developed in Task 9B-1 and 9B-2 and perform predictive modelling of penetration profiles of Na-22, Cl-36, Ni-63, Ba-133, and Cs-137 in the rock cores (A4, A11, A13, D15, and D16). A set of data that is already reported for these cores, relating to Cs-137 surface activities, could be used as input to the modelling (Löfgren and Nilsson 2020).

1.3 Scope and limitations

The modelling in Task 9B is based on the conventional matrix diffusion model. Matrix diffusion in A- and D-cores is modelled accounting for retardation by linear sorption. No surface sorption was invoked for transport in the rock matrix. Ion exclusion effect for chloride was considered. In this conventional matrix diffusion model, the rock was assumed to be a homogeneous porous medium with regard to diffusivity and sorption. Porosity and sorption distribution coefficient were set to be constant.

In Task 9B-3, predictions of tracer distribution profile were made based on the conventional matrix diffusion model using mainly experimentally determined parameters and where the measured activities in the circulating solution were chosen as boundary condition.

1.4 Outline of the calculations

Chapter 3 shows activity balances for the most important radionuclides. In the balance for each species, the injected tracer is compared with the activity in the rock matrix, activity in the reservoir, other identified loss and non-identified loss.

Since the loss of activity in the system is important, it is not possible use a simple balance to determine the activity in the reservoir as a function of time. Therefore, an analytical expression was fitted to the activity in the reservoir as a function of time (Section 4.1).

In Section 4.2, using data taken from the Task 9B Description and other available reports, predictions were done for the activity profile in the rock matrix for some radionuclides and compared with the experimental profiles.

In Section 4.3, the experimental profiles are fitted using the diffusion sorption model, Equation 2-2, where two parameters are fitted; the effective diffusivity and the capacity factor. The experimental values were compared with values calculated by integration along the slice length. Both parameters were fitted for each nuclide in each core.

2 Methodology and model

Figure 1-1 shows the layout of the experiment and the locations of the drilled cores (Nilsson et al. 2010). The experimental system is composed of reservoir and rock matrix. The reservoir contains the solution with the different tracers, which are in contact with the rock in two locations: stub section, where the A-cores are located, and the slim hole with the D-cores. In both sections of the reservoir, the solute activity is kept identical and evolves with time. Solute enters the rock matrix from the reservoir. In both A- and D-cores, solute is transported by molecular diffusion and may be retarded by sorption. Linear diffusion takes place in A-cores and radial diffusion takes place in the D-cores. However, because of the limited penetration distances also the latter is modelled as linear diffusion.

2.1 Mass Balance

In general, it may be expected that the tracers injected were found in the circulating water and within the rock matrix. However, some tracers were found sorbed in other parts of the equipment (PEEK tubes, epoxy resin). Therefore, the first step was to perform a mass balance for the tracers in the cocktail solution. The tracers at the termination of experiments were found in the following locations:

1) Within the rock matrix.
2) In the reservoir.
3) Tracers attached to PEEK plate, epoxy resins, sorbed in PEEK tubing, and dissolved in the mixing of epoxy resin and isopropanol slurry.
4) A fraction of the tracers was removed from the reservoir for analyses.

The activity in a given core is calculated by adding the activity in the slices of that core. The total activity may then be determined in the A-cores and the D-cores. The total activity in the stub zone where the A-cores are located is then calculated as

$$\text{Activity in the stub zone} = [\text{Total activity in A cores}] \cdot \frac{\text{Cross section stub zone}}{\text{Cross section A cores}}$$

Similar procedure is used for the Activity in the slim hole zone where the D-cores are located.

The items 3) and 4) are considered as identified loss. The difference between the injected activity of the tracer and the sum of the tracer within the matrix, in the reservoir and the identified loss is called Not-identified loss.

In determining the tracers within the rock matrix, it should be noted that the provided tracer amounts in the rock matrix are incomplete, since only fraction of the affected rock mass was cored and analysed. To determine the total amount of activity that has diffused into the rock is assumed that the mean value of activity per cross section area for the A-cores is similar to that found in the rock where the A-cores were located. The same is applied for the D-cores.

2.2 Boundary concentration curve fitting

The activity of the circulating solution is given at different times along the experiment. For the purpose of incorporating these measured activities in the modelling; a function is fitted to these experimental data. The resulting function was applied as boundary condition in the simulations.

The tracer activity of the cocktail evolves with time when nuclides diffuse into the rock or are sorbed on the tubes or other parts of the system. Since the activity of the sorbing nuclides in the reservoir decreases very rapidly at short times and is almost flat at long times, the following relationship is fitted:

$$\frac{c_b}{c_{b,0}} = P_a\, e^{(-P_b * t)} + P_c\, e^{(-P_d * t)} + P_e \tag{2-1}$$

where t is the elapsed time in hours, P_a (–), P_b (1/h), P_c (–), P_d (1/h), and P_e (–) are constant. c_b is the boundary activity (Bq/mL) and $c_{b,0}$ is the activity in the reservoir at 0 hours (Bq/mL).

For each tracer, the five parameters were determined by fitting. This function was then used as boundary condition in the modelling.

2.3 Rock matrix diffusion model

Since the experimental data are reported corrected for decay the diffusion-sorption equation for solute is established without considering decay,

$$\alpha_p \frac{\partial c_f}{\partial t} = D_e \frac{\partial^2 c_f}{\partial x^2} \tag{2-2}$$

with

$$\alpha_p = (\varepsilon + K_d \rho) \tag{2-3}$$

where α_p is the capacity factor (–); c_f indicates aqueous solute activity (Bq/mL); D_e effective diffusivity of the tracer in the rock matrix (m^2/s); ρ is bulk rock density (kg/m^3); K_d sorption constant (m^3/kg); ε the porosity (–).

The initial and boundary conditions to Equation (2-2) are written as follows,

$$c_f(x, t = 0) = 0 \tag{2-4}$$

$$c_f(0, t) = c_b(t) \tag{2-5}$$

$$c_f(x \to \infty, t) = 0 \tag{2-6}$$

For solving Equations (2-2) to (2-6), the numerical inversion of Laplace transform was used. The parameters D_e and α_p were fitted to measured activity profile in rock matrix.

The aqueous solute activity in the rock matrix (c_f, Bq/mL) as a function of penetration depth cannot be compared directly with the experimental activity in the slice, which is expressed as activity per mass (Bq/g). Therefore, the activity in a slice is calculated by integrating the activity (in the porewater and sorbed on the rock matrix) in the slice and dividing by the slice mass. This value may then be compared with the experimental mean activity in respective slice.

2.4 Inverse modelling for the Tasks 9B-1 and 2

The activity profiles in the cores are found in the Delivery 33; Updated information on core concentrations in LTDE-SD, June 13, 2019. The experimental values were compared with values calculated by integration along the slice length. Capacity factor and effective diffusion coefficient were fitted for each nuclide in each core.

2.5 The predictive modelling in Task 9B-3

Predictive modelling in Task 9B-3 was only applied to ^{137}Cs. We make the predictions in two levels:

- In level one, we used the γ-spectrometry data Nilsson et al. (2010). For effective diffusivity coefficient we used the values given by SKB Nilsson et al. (2010). The value of the capacity factor is determined from the activity in the respective core. The real reservoir activity is used as boundary condition.
- In level two, we used the γ-spectrometry data Nilsson et al. (2010). In this case the sorption constant was determined from the concentration in the first slice, and the effective diffusion coefficient is determined from the activity in the respective core determined by γ-spectrometry.

In this sub-task, the same diffusion-sorption equation, i.e. Equation (2-2), was set-up. We applied Laplace transform method together with initial and boundary conditions, the analytical solution to Equation (2-2) in Laplace domain is written as,

$$\bar{c}_f = \bar{c}_b \exp\left(-\sqrt{\frac{\alpha_p s}{D_e}}\, x\right) \tag{2-7}$$

with

$$\bar{c}_b = c_{b,0}\left(\frac{P_a}{P_b + s} + \frac{P_c}{P_d + s}\right) \tag{2-8}$$

where s is the Laplace variable (T^{-1}).

The analytical Laplace solution, Equation (2-7), was applied to make predictions of transient solute concentration in rock matrix, combined with numerical inverse Laplace transform method (de Hoog et al. 1982) in both levels.

3 Tracer mass balance verification

The detailed data are listed in Table 3-1 and the tracer distribution is presented in Figure 3-1.

Table 3-1. Activity distribution in Task 9B based on experimental data.

Tracer	Tracer injected (MBq)	Rock matrix (MBq)	Reservoir (MBq)	Identified loss (MBq)	Non-identified loss (MBq)
Na-22	3.80	0.03	2.82	0.71	0.24
Co-57	18.90	0.99	0.16	9.68	8.08
Ba-133	1.78	0.22	0.99	0.36	0.22
Cs-137	8.80	3.26	2.79	1.01	1.74
Cd-109	27.10	2.00	4.14	4.65	16.31
Ag-110m	0.47	0.06	0.00	0.29	0.12
Gd-153	4.30	0.25	0.01	1.39	2.65
Cl-36	5.90	0.00	4.93	0.94	0.03
Ni-63	30.40	1.92	7.59	2.14	18.75
Ra-226	0.15	0.05	0.06	0.01	0.03
Np-237, ng	3.14E+05	7.39E+03	1.61E+05	1.12E+05	3.39E+04

In Figure 3-1, we found that for non-sorbing and weakly-sorbing tracers, i.e. Na-22 and Cl-36, their mass balance is acceptable. In both cases, the location of more than 95 % of the injected tracer is identified at the termination of experiments. The largest part of the recovered tracers is found in the reservoir, which agrees well with our expectations. However, we may notice that a significant portion of tracers, even larger than the amount in rock matrix, is categorized as “identified loss”. This is mainly caused by the sampling loss from the reservoir during experiments.

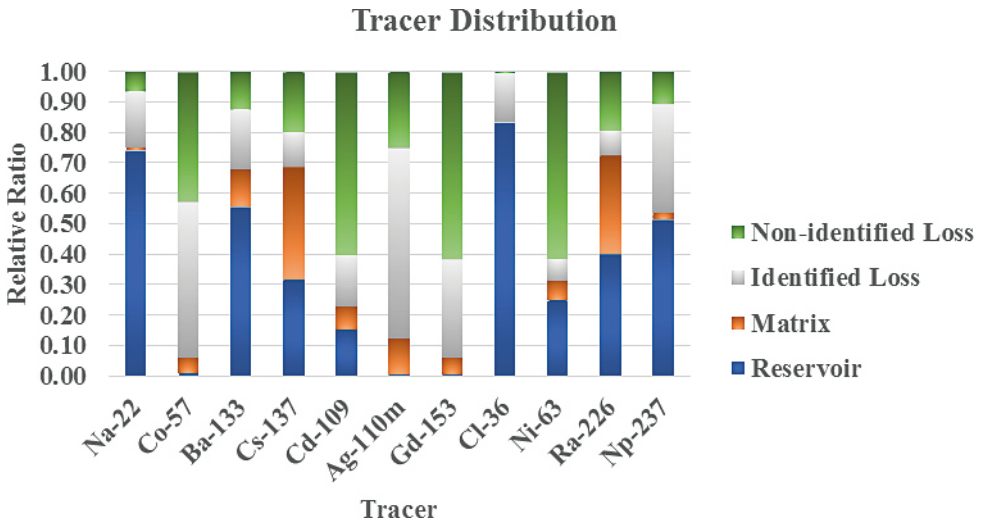

Figure 3-1. *Tracer distribution in Task 9B at the termination of experiments. The sum of tracer amount is normalized to unity.*

For strongly-sorbing tracers, the performances are different based on seemingly two sorption mechanisms. For cation-exchange tracers, i.e. Ba-133, Cs-137 and Ra-226, the mass balance verification is rather acceptable since around 80 % of the tracer is identified. For these analysed tracers, most were observed in the reservoir and rock matrix as expected. However, the amount of the tracer in the reservoir and the rock matrix is only about 70 %. The “Identified loss” amount is smaller, mainly resulting from the sampling loss.

In contrast, the mass balance verification of surface complexation ions is rather bad, especially for Co-57, Ni-63, Cd-109 and Gd-153. A significant portion of tracers, compared with those in the reservoir and rock matrix, is categorized as “Identified loss”; which are mainly discovered in PEEK-epoxy plate and PEEK tubing. But, more importantly, we failed to account for more than half of the injected tracer, called the non-identified portion.

4 Simulation results

4.1 Variation of activity with time in circulating solution, fitting of the experimental data

As described, Equation (2-1) was used to reproduce measured curves for the determination of best-fit parameters. Obtained coefficients using the least square method are presented in Table 4-1.

Table 4-1. Best-fit parameters used in Equation (2-1) for describing time-dependent boundary condition.

Tracer	P_a (–)	P_b (1/hr)	P_c (–)	P_d (1/hr)	P_e (–)	Init. Act, Bq/mL
Na-22	9.9212E−2	1.7378E−3	3.5024E−2	2.3663E−1	8.6512E−1	3250
Cl-36	−4.015E−0	2.4281E−1	4.1135E+0	2.4647E−1	9.0124E−1	5670
Co-57	5.1223E−1	2.2496E−2	4.8148E−1	3.3355E−1	6.3136E−3	18300
Ni-63	2.4600E−1	3.9215E−4	5.0037E−1	2.9030E−1	2.5082E−1	28800
Ba-133	1.9204E−1	4.6572E−4	2.2440E−1	2.5998E−1	5.5711E−1	1730
Cs-137	3.0561E−1	1.6425E−3	3.4438E−1	2.7936E−1	3.4479E−1	8460
Cd-109	2.2965E−1	3.3911E−4	6.6635E−1	1.6915E−1	1.1140E−1	25960
Ra-226	1.5599E−1	1.9830E−3	4.4766E−1	5.1749E−1	3.9625E−1	145

Fitted curves can be found in Appendix A. In general, a well agreement is found between the experimental and the fitted values. Several tracers show very fast decrease of the activity at very short time. This high decrease rates may be mainly attributed a sorption on the surface of the reservoir, including the tubing and other materials. Co-57 shows an extreme decrease rate, more than 99 % disappearing in a few days. The initial activity (last column) correspond to the extrapolation to 0.0 hours. These values are included, since the agreement is not good when the initial activity is calculated from experimental values. For Na-22, 3.2 MBq are injected in a volume of 1 150 mL (Löfgren and Nilsson 2020). This corresponds to an initial activity of 2 783 Bq/mL, which is very different of the value 3 200 Bq/mL indicated as the activity at 2 hours (Löfgren and Nilsson 2020).

4.2 Predictive modelling

In this section, the activity profiles for the nonsorbing species Cl-36 and the sorbing species Na-22, Ba-133, and Cs-137 are predicted using effective diffusivities and capacity factors determined from data found in SKB reports (Nilsson et al. 2010, Widestrand et al. 2010a, b). The predicted activity profiles are compared with the experimental values for one core for each species.

The used values for *the* capacity factor, α_p (–); the effective diffusivity of the tracer in the rock matrix, D_e (L^2T^{-1}); the bulk rock density, ρ (ML^{-3}); the sorption constant, K_d (L^3M^{-1}); and the porosity, ε (–). Are shown in Table 4-2.

Table 4-2. Parameters values used in the simulations.

Species	Sorption[2] constant, K_d, (m^3/kg)	Matrix[1] porosity, ε (–)	Rock[1] formation factor F_f (–)	Effective diffusivity, D_e, (m^2/s)	Rock[3] Density, (kg/m^3)
Chloride, Cl-36	0.0	0.0021	2.2E−05	4.4E−14	2660
Sodium, Na-22	2.9E−04	0.0021	2.2E−05	4.4E−14	2660
Barium, Ba-133	2.1E−03	0.0021	2.2E−05	4.4E−14	2660
Caesium, Cs-137	2.2E−02	0.0021	2.2E−05	4.4E−14	2660
Niquel, Ni-63	1.5E−02	0.0021	2.2E−05	4.4E−14	2660
Cadmiun, Cd-109	5.1E−03	0.0021	2.2E−05	4.4E−14	2660
Radium, Ra-226		0.0021	2.2E−05	4.4E−14	2660

[1] (Nilsson et al. 2010, Table 4-1.)
[2] (Nilsson et al. 2010, Table 4-2.)
[3] (Widestrand et al. 2010a, p 12.)

The agreement between the predicted and experimental values is not good, large differences are generally found. Results for some cores are shown in Figures 4-1 and 4-2 for the non-sorbing species Cl-36 and the sorbing species Na-22, Ba-133, and Cs-137 respectively. Only a core is shown for each species, since the bad agreement is similar for the different species. In general, the effective diffusivity used in the predictions is lower than the real effective diffusivity found in the different samples.

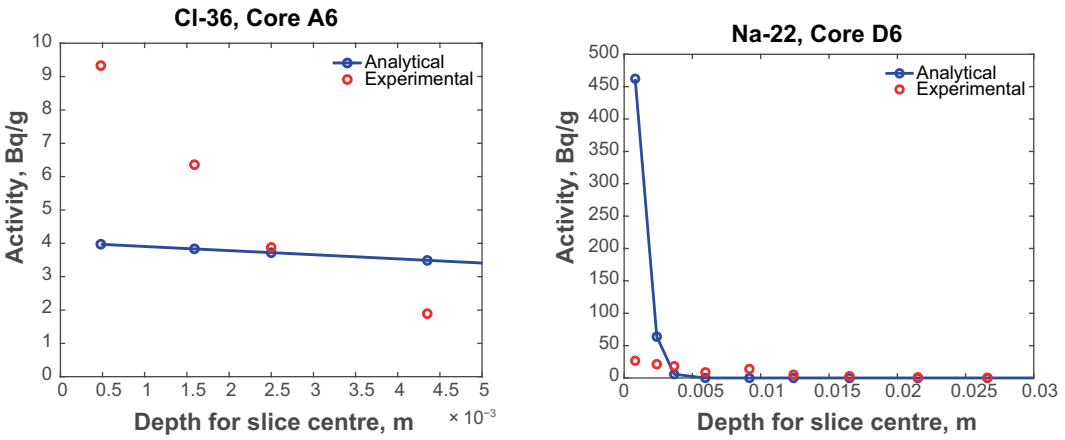

Figure 4-1. Predicted and experimental values for Cl-36 – Core A6 and for Na-22 – Core D6.

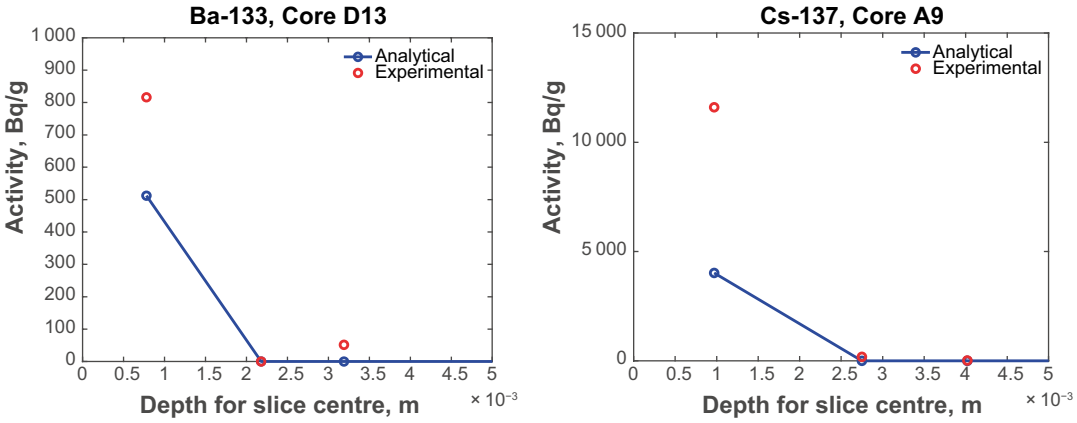

Figure 4-2. Predicted and experimental values for Ba-133 – Core D13 and for Cs-137 – Core A9.

4.3 Task 9B-1 and 2 – Inverse modelling

The model considers that the rock is totally homogeneous, therefore the same value is assumed for the effective diffusivity and capacity factor for the respective species and respective core. The activity profile is fitted to the experimental activity profile.

Since the number of fitting is very high, only a couple of figures are show, in which the experimental data is compared with the fitted curves. Figure 4-3 (left) shows the comparison between experimental and fitted values for the Core A6 for Caesium. The data of Barium for the Core D12 is compared in Figure 4-3 (right).

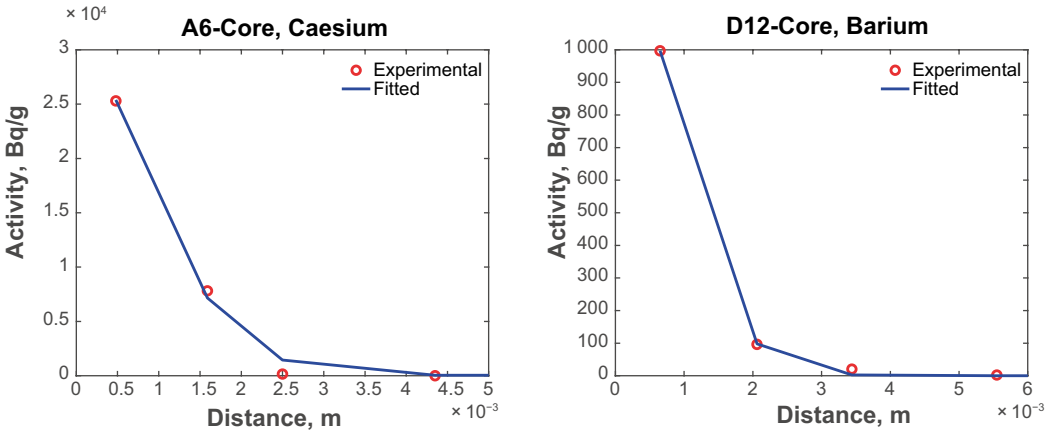

Figure 4-3. *Comparison between experimental data and fitted values: (left) Core A6 for the tracer Caesium and (right) Core D12 for the tracer Barium.*

4.3.1 Fitting for the non-sorbing species Cl-36

For the non-sorbing species Cl-36, 11 cores were in total analysed (6 A-cores and 5 D-cores). The core A13 was not analysed for Cl-36, since activities for the 2nd and 3rd slices are missing and the following values are too low. The results are presented for both cores types. Figure 4-4 shows histograms for the effective diffusivity (in log-scale) and the capacity factor. For effective diffusivity the values are distributed in about two orders of magnitude. The relationship between effective diffusivity and capacity factor is shown in Figure 4-5. In general, the capacity factor and the effective diffusivity are concentrated in the lower values respectively. The effective diffusivities and capacity factors for all the analysed cores are shown in Appendix B1. The statistics for these parameters are:

Entity	Log(De)	Alpha
Mean	−14.79	0.0037
Stdev	0.65	0.0032
Min	−15.43	0.0003
Max	−13.44	0.0104

The obtained effective diffusivities are small, with a mean value of 1.6E−15 m^2/s, much lower than for the sorbing tracers. This may partially be explained by the anion exclusion effect. However, the variation interval of the effective diffusivity is very large, two orders of magnitude. But the most of the values are located at the lower interval, −15.4 to −14.4.

The capacity factor for non-sorbing nuclides is equivalent to the porosity. It is noted that porosity for the Cores A is higher than the porosity of Core D. The average porosity is 0.0037 with the most of the values located in the lower value interval.

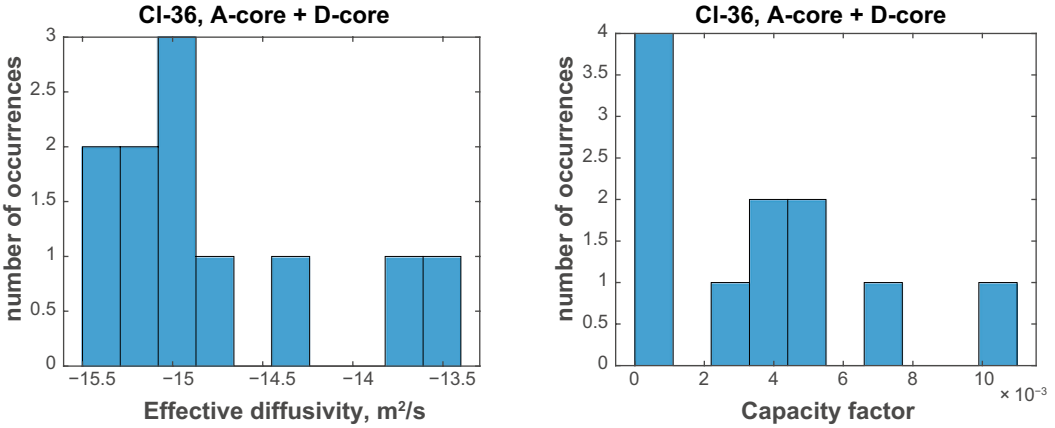

Figure 4-4. *Histogram showing the effective diffusivity and capacity factor for both core types.*

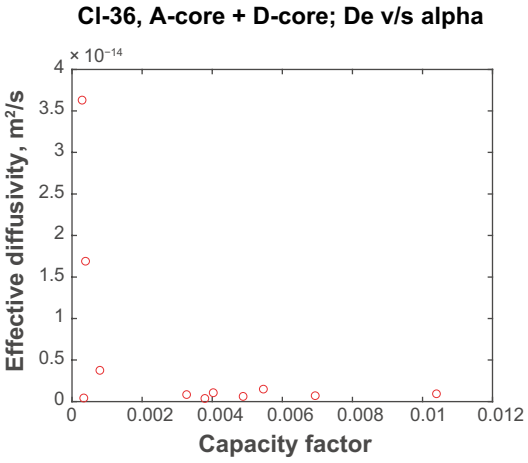

Figure 4-5. *Effective diffusivity versus capacity factor for both core types.*

4.3.2 Fitting for the weakly sorbing species Na-22

For the weakly sorbing species Na-22, 22 cores were in total analysed (12 A-cores and 10 D-cores). The core A13 was not analysed for Na-22, since activities for the 1st slice is given with large uncertainty. The results are presented for both cores types. Figure 4-6 shows histograms for the effective diffusivity (in log-scale) and capacity factor. The relationship between effective diffusivity and capacity factor is shown in Figure 4-7. The effective diffusivities and capacity factors for all the analysed cores are shown in Appendix B2. The statistics for these parameters are:

Entity	Log(De)	Alpha
Mean	−13.42	0.0302
Stdev	0.36	0.0233
Min	−13.97	0.0085
Max	−12.82	0.0906

The average diffusion coefficients are very similar for cores (A-core and D-core). The mean value for the effective diffusivity is 3.8E−14 m^2/s. The values of the capacity factor are very small, which indicates a very low sorption constant, 1.1E−05 m^3/kg.

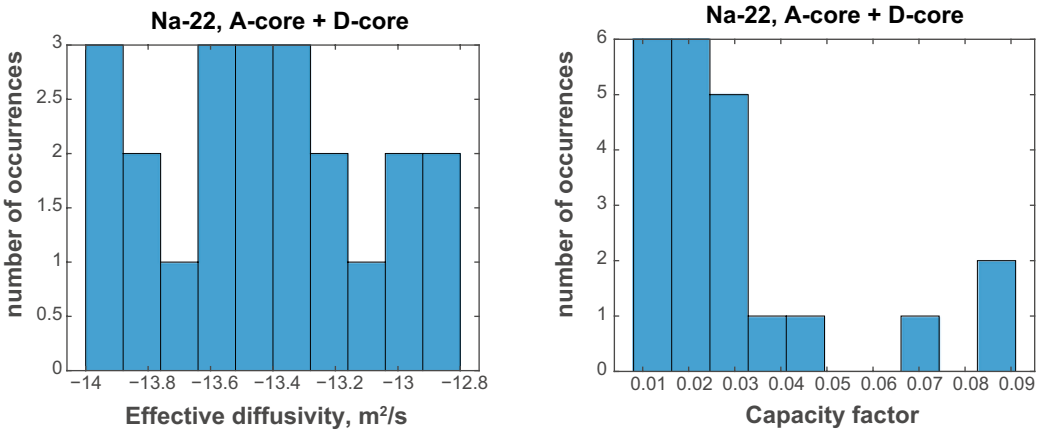

Figure 4-6. *Histogram showing the effective diffusivity and capacity factor for both core types.*

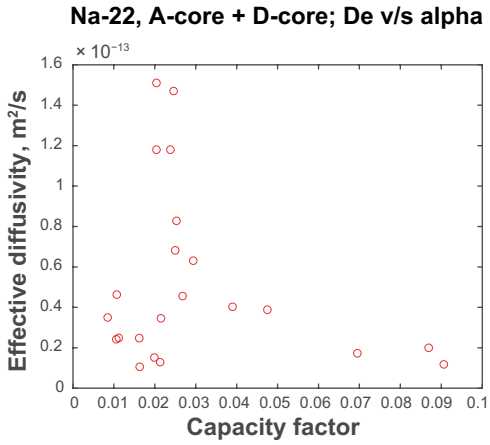

Figure 4-7. *Effective diffusivity versus capacity factor for both core types.*

4.3.3 Fitting for the sorbing species Ba-133

For the sorbing species Ba-133, 23 cores were in total analysed (13 A-cores and 10 D-cores). The results are presented for both cores types. Figure 4-8 shows histograms for the effective diffusivity (in log-scale) and capacity factor. The relationship between effective diffusivity and capacity factor is shown in Figure 4-9. The effective diffusivities and capacity factors for all the analysed cores are shown in Appendix B3. The statistics for these parameters are:

Entity	Log(De)	Alpha
Mean	−12.90	3.45
Stdev	0.29	1.78
Min	−13.50	0.90
Max	−12.10	7.55

The mean value for the effective diffusivity is 1.3E−13 m^2/s. The value of the capacity factor is 3.45, typical value for species with intermediary sorption, which indicates a sorption constant of 0.0013 m^3/kg.

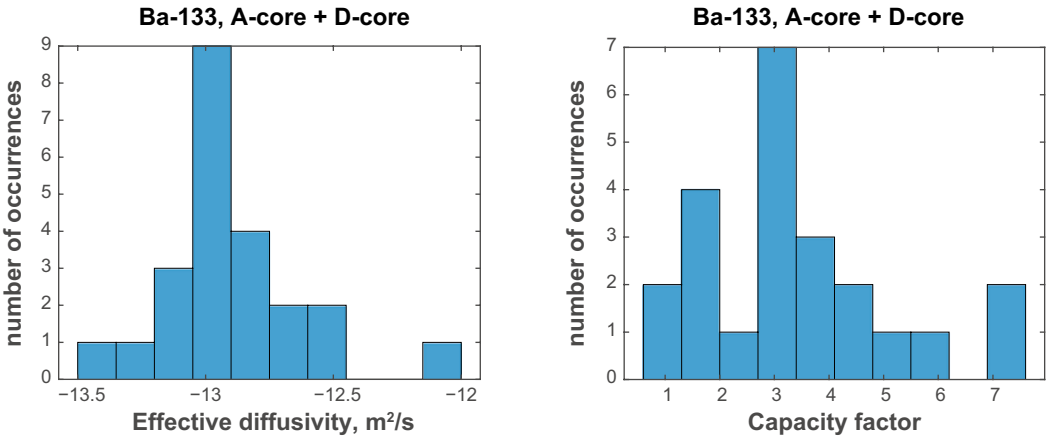

Figure 4-8. *Histogram showing the effective diffusivity and capacity factor for both core types.*

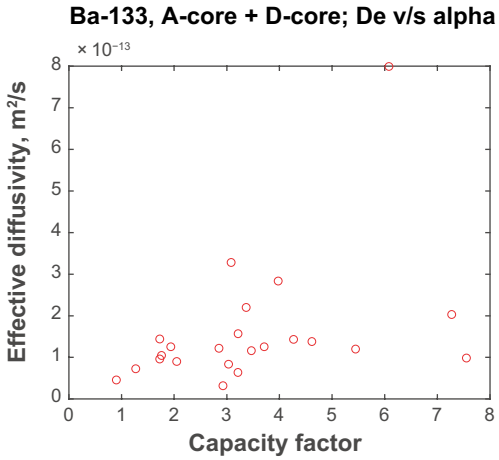

Figure 4-9. *Effective diffusivity versus capacity factor for both core types.*

4.3.4 Fitting for the sorbing species Cs-137

For the sorbing species Cs-137, 23 cores were in total analysed (13 A-cores and 10 D-cores). The results are presented for both cores types. Figure 4-10 shows histograms for the effective diffusivity (in log-scale) and capacity factor. The relationship between effective diffusivity and capacity factor is shown in Figure 4-11. The effective diffusivities and capacity factors for all the analysed cores are shown in Appendix B4. The statistics for these parameters are:

Entity	Log(De)	Alpha
Mean	−12.24	18.06
Stdev	0.31	8.60
Min	−12.77	7.72
Max	−11.55	35.9

The effective diffusion coefficient for Cs-137 is 5.8E−13 m^2/s. The mean capacity factor is some lower than the expected value (about 58.5). The mean value, 18.1, corresponds to a sorption constant of 0.0068 m^3/kg. The expected value was 0.022 m^3/kg.

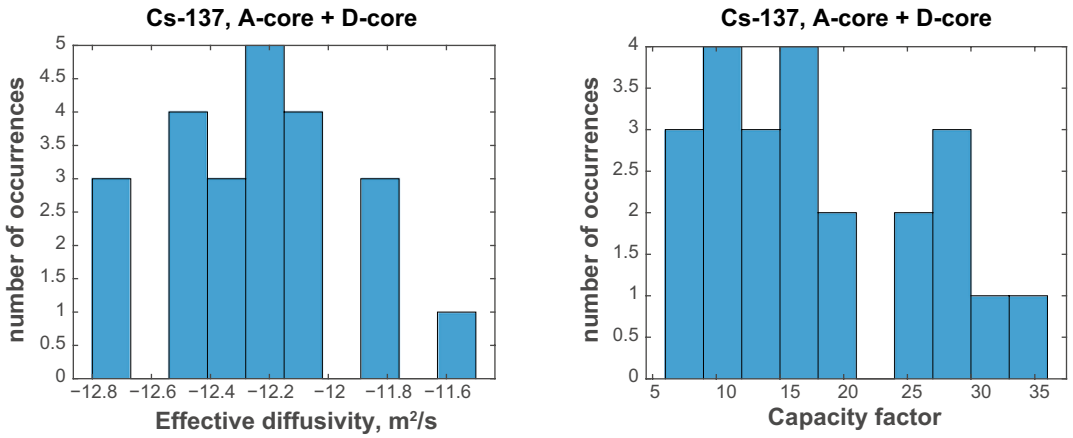

Figure 4-10. *Histogram showing the effective diffusivity and capacity factor for both core types.*

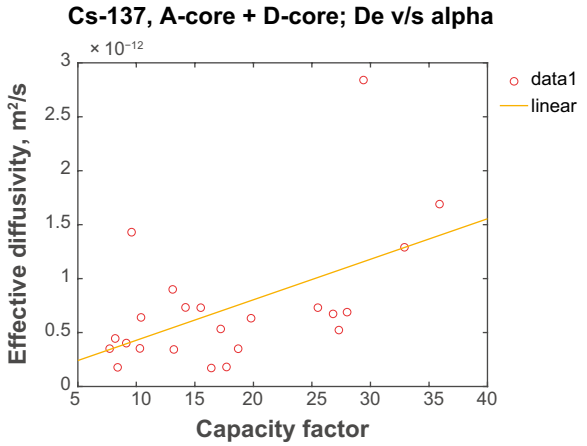

Figure 4-11. *Effective diffusivity versus capacity factor for both core types.*

4.4 Task 9B-3 – Predictive modelling

4.4.1 Level one

In these predictions, we use the γ-spectrometry data, which indicate the activity distribution for the tracer Cs-137 (Figure 3-3 for A-cores and Figure 3-6 for D-cores in Nilsson et al. (2010)), as input to the modelling. The data in the figures show the approximated amount of activity in each of the A-cores and D-cores, measured in 24 mm-diameter cylinders before slicing. The penetration profile determined from the activity that has penetrated the core could be estimated by varying the diffusion coefficient and the sorption constant. But, since we have only a value to fit, the total activity that has penetrated the core, the diffusion coefficient given in Nilsson et al. (2010) is used. Therefore, the value for the sorption constant is obtained.

The approximate activity for the target cores is shown in Table 4-3. The values for diffusion coefficient, rock density, and the porosity used in these predictions are those shown in Table 4-4 (Nilsson et al. 2010). The values obtained for the sorption constant are shown in Table 4-5.

Table 4-3. Activity measured in the target cores, approximate value.

Sample	Activity interval (1E+04 Bq)	Mean activity (1E+04 Bq)
A4	1–2	1.5
A11	1–2	1.5
A13	2–3	2.5
D15	2–2.5	2.25
D16	2–2.5	2.25

Table 4-4. Diffusion coefficient, rock density, and porosity used in the predictions.

Entity	Value
Diffusion coefficient (m^2/s)	2.20E−11
Density (kg/m^3)	2660
Porosity (–)	2.10E−3

Table 4-5. The fitted parameter of K_d for Caesium in each core.

Sample	K_d (m^3/kg)
A4	0.066
A11	0.066
A13	0.184
D15	0.148
D16	0.148

4.4.2 Level two

In the prediction in level one, the diffusion coefficient given by the experimentalist (Nilsson et al. 2010) was used and the sorption constant was determined using the surface activity distribution of Caesium in A- and D-cores. However, the values for sorption coefficient obtained in these predictions were too large compared with the values given in Nilsson et al. (2010), therefore we try to improve the prediction by determining the sorption coefficient using the activity in the first slice and the reservoir activity at the end of the experiment. For this, we used the cores with known activity belong to the same category in the figure showing γ-spectrometry results (Figure 3-5 in Nilsson et al. 2010). For example, for cores A4 and A11, the experimental activities in the first slice in cores A5, A10, and A17 were used to determine the sorption constant. This is considered a reasonable approximation due to the fact that the first slice is very thin and the reservoir activity remained constant for more than 120 days around the final value. Therefore, we could assume that quasi-equilibrium is obtained

between the activity in the reservoir and the rock activity in the first slice. With knowing reservoir activity and activity in the first slice, approximate sorption constant is estimated. Thereafter effective diffusivity is calculated. There both parameters are obtained. Parameters used for predictions are presented in Table 4-6.

Table 4-6. Parameters used in the predictions.

Core No.	K_d (m³/kg)	D_e (m²/s)
A4/A11	1.54E−3	1.99E−12
A13	3.04E−3	2.73E−12
D15/D16	6.00E−3	2.16E−12

We compared the predicted distribution profiles of level one and two with known experimental data in Figure 4-12. It indicates that the level two is better than level one since the penetration depth in level one case is too short and the activity close to the border is very high. Noticeably, most points in the tails for experimental results were discarded or discussed in this report. The reason is that those data points not only make a minor contribution to analysis but also may not be reliable, since contamination and detection limits also play significant roles in measurements. To facilitate the analysis, we only focus on the data points related to dominant mechanisms in this report. The fitting was done using the totality of the data points for the respective cores.

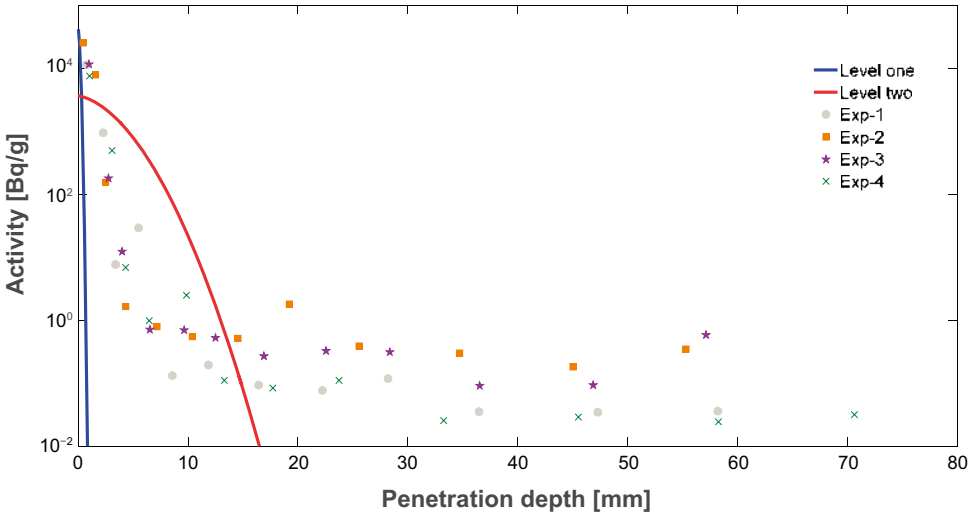

Figure 4-12. *Comparison between predicted penetration profiles in level one and two with obtained experimental data.*

5 Discussion

The experimental activity profiles show an anomalous behaviour, in particular for the sorbing tracer Cs-137. The profiles show a reasonable diffusion in the region close to the surface and suggest a very high diffusion in the inner region. When these profiles were fitted by using the diffusion-sorption model, the diffusion coefficient in the inner region is higher than that in free water; i.e., about three orders of magnitude. We try to find the probable reasons that could result in these profiles. However, at present, many of these values, located at deeper locations, were removed since in some cases, these values were below or very close to the detection limit. Possible contamination was also other reason.

We keep here some of the possible reasons that may modify the diffusion results, since they could be useful in other situations:

1) Capillarity caused by drying at the surface: Tracers might be transported by capillary movement of the pore water caused by drying in the surface, which could have taken place before core drilling. This may provide capillary forces from the slim hole to the outer surface of the large diameter core for the D-cores resulting the long tailing of tracer distribution profiles in D-cores. However, this interpretation is not applicable to A-cores since the possible drying takes place at the front of the rock where the A-cores are drilled and the capillary forces act toward the A-cores surface; i.e. towards the surface exposed to reservoir, therefore this mechanism cannot be applied to explain the long tailing in A-cores.

2) After-diffusion process: The diffusion process is likely to continue after the termination of the experiment. However, it is still an open question whether this after-diffusion can cause the unexpected profiles or not. Löfgren and Nilsson (2020) made a spot check of Na-22 and Cs-137 penetration in two samples of A12 and A6, which were sliced in November 2007 and February/March 2008, respectively. Some differences are observed, but they are taken from two different cores, thus it is not possible get some conclusions about this effect due to the heterogeneities characteristic of this kind of rock.

3) Existence of negatively charged nuclide in pore water: In the Table 3-3 of (Widestrand et al. 2010b), from speciation studies for Co-57, is found around 70 % of Co-57 is as $HCoO_2^-$ in water. Thus, a portion of Co-57 tracer might diffuse into rock matrix without being sorbed. For this reason, the penetration depth of Co-57 could be longer than the expected and could explain the long tails. However, the mechanisms are complex, since a fraction of $HCoO_2^-$ in the pore water that diffused into the rock matrix may re-equilibrate to Co^{2+}, which will be sorbed in the rock. On the other hand, the Co^{2+} in the pore water where the Co-57 was sorbed may be decomposed in two fractions; $HCoO_2^-$ and Co^{2+}. Then a part of the Co-57 sorbed in the rock close to the surface will be desorbed and will diffuse into the rock matrix without be sorbed. In one first approximation, we can say that we always find $HCoO_2^-$ and Co^{2+} in the pore water, in proportions given by the speciation. Many factors would be controlled before to get a definitive conclusion. Other nuclides, in which this mechanism could be active are Ag-110 and Cd-109. However, it cannot explain the long tails in other tracers.

4) Non-uniform distribution of sorption sites in rock matrix: The autoradiography of selected samples in Figure 3-15 and Figure 3-22 in Nilsson et al. (2010), indicates that the distribution of sorption sites is not uniform. For this reason, it is probable to find special pathways, in which sorption effects are smaller or marginal. Due to this, a fraction of the sorbing tracers might penetrate deeper into the rock matrix, while other tracers will be sorbed close to the surface at the inlet. As a result, a longer tailing would result at the termination of experiment. However, the contribution is not enough to explain the actual activity profiles.

6 Conclusion

The following conclusions are obtained from these simulations:

The mass balance shows that for the most of the injected tracers, in particular for the strongly sorbing, the amount of tracer that is lost from the system at the end of the experiment is important or very important, in many cases around 50 %. Therefore, we cannot assume that the system is closed and that the reservoir activity can be estimated by mass balance assumption.

The results of the inverse modelling (fittings) are shown in Table 6-1, for the effective diffusion coefficient. Table 6-2 shows the results for the capacity factor. For the effective diffusion coefficient, the values from the fitting process were similar for Na-22, slightly higher for Ba-133 and higher for Cs-137. The value for Cs could be due to surface diffusion that may takes place for Cs.

For the capacity factor the values obtained for fitting were slightly lower that the values of the literature. These relative higher literature values might be caused by the increase of specific surface area in performed batch sorption experiments (Widestrand et al. 2010a).

Table 6-1. Effective diffusion coefficient, m^2/s, for the tracers used in the fitting process.

Species	Fitted Effective Diffusion Coef., m^2/s		Literature data[1], m^2/s
	Interval, m^2/s	Median, m^2/s	
Cl-36	(0.004–0.36) E−13	0.04 E−13	
Na-22	(0.1–1.5) E−13	0.4 E−13	0.4 E−13
Ba-133	(0.3–8.0) E−13	1.0 E−13	0.4 E−13
Cs-137	(1.7–28.0) E−13	5.0 E−13	0.4 E−13

[1] The data were taken from Widestrand et al. (2010a).

Table 6-2. Capacity factor for the tracers used in the fitting process.

Species	Fitted Effective Diffusion Coef., m^2/s		Literature data[1], m^2/s
	Interval, m^2/s	Median, m^2/s	
Cl-36	(0.0003–0.001)	0.004	
Na-22	(0.009–0.09)	0.03	0.27–1.0
Ba-133	(0.9–7.6)	3.0	5.3–27
Cs-137	(8.4–36)	17.0	27–266

[1] The data were taken from Widestrand et al. (2010a).

- In Task 9B-3, we estimated the distribution profile in Core A4, A11, A13 and D15, D16. We used the γ-spectrometry data and the effective diffusivity coefficient given by SKB (Nilsson et al. 2010). The most reasonable predictions were those using the γ-spectrometry data and the sorption constant determined from the first slice assuming equilibrium with the activity in the reservoir at the end of the experiments.

References

SKB's (Svensk Kärnbränslehantering AB) publications can be found at www.skb.com/publications.

De Hoog F R, Knight J H, Stokes A N, 1982. An improved method for numerical inversion of Laplace transforms. SIAM Journal on Scientific and Statistical Computing 3, 357–366.

Löfgren M, Nilsson K, 2020. Task description of Task 9B – Modelling of LTDE-SD performed at Äspö HRL. Task 9 of SKB Task Force GWFTS – Increasing the realism in solute transport modelling based on the field experiments REPRO and LTDE-SD. SKB P-17-30, Svensk Kärnbränslehantering AB.

Nilsson K, Byegård J, Selnert E, Widestrand H, Höglund S, Gustafsson E, 2010. Äspö Hard Rock Laboratory. Long term sorption diffusion experiment (LTDE-SD). Results from rock sample analyses and modelling. SKB R-10-68, Svensk Kärnbränslehantering AB.

Widestrand H, Byegård J, Selnert E, Skålberg M, Höglund S, Gustafsson E, 2010a. Long term sorption diffusion experiment (LTDE-SD). Supporting laboratory program – Sorption diffusion experiments and rock material characterisation. With supplement of adsorption studies on intact rock samples from the Forsmark and Laxemar site investigations. SKB R-10-66, Svensk Kärnbränslehantering AB.

Widestrand H, Byegård J, Nilsson K, Höglund S, Gustafsson E, Kronberg M, 2010b. Long term sorption diffusion experiment (LTDE-SD). Performance of main in situ experiment and results from water phase measurements. SKB R-10-67, Svensk Kärnbränslehantering AB.

Appendix A

The experimental activity and the fitted curves for the activity of the species in the reservoir are shown in Appendix A.

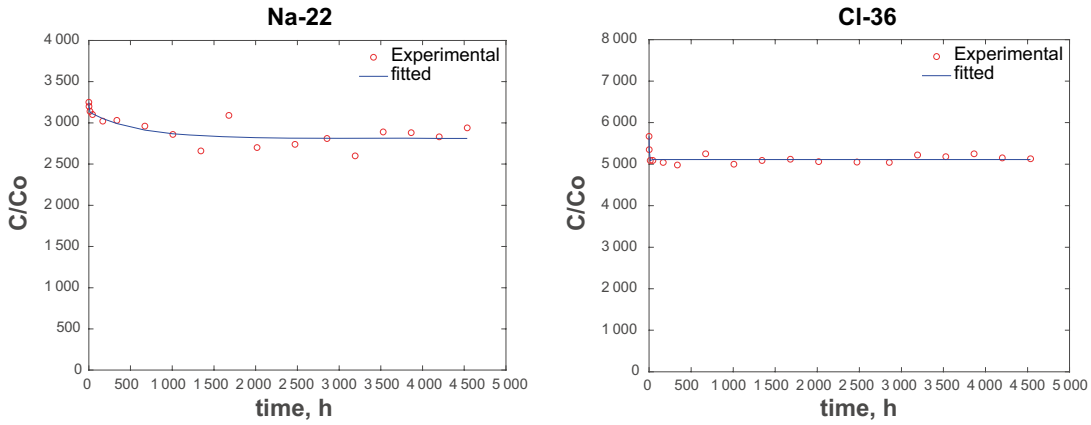

Figure A-1. *Activity of Na-22 and Cl-36 in the reservoir as a function of time; experimental and fitted values.*

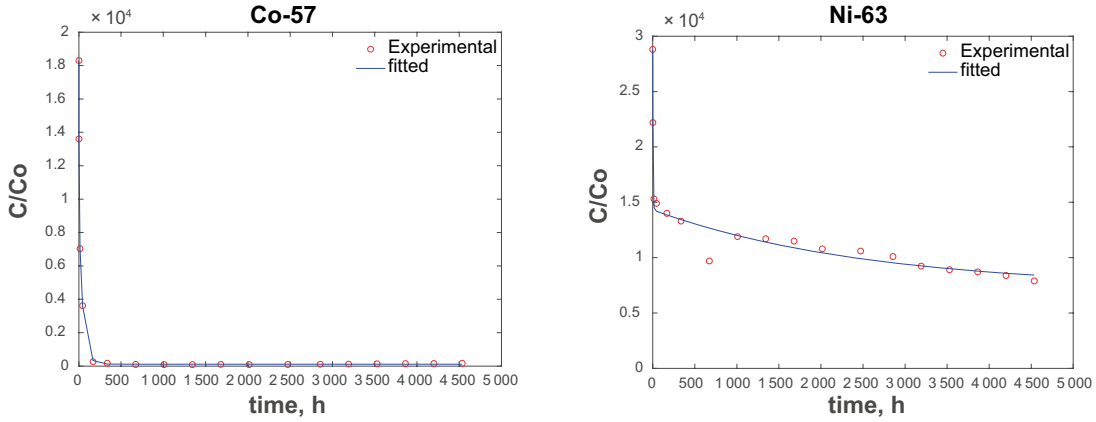

Figure A-2. *Activity of Co-37 and Ni-63 in the reservoir as a function of time; experimental and fitted values.*

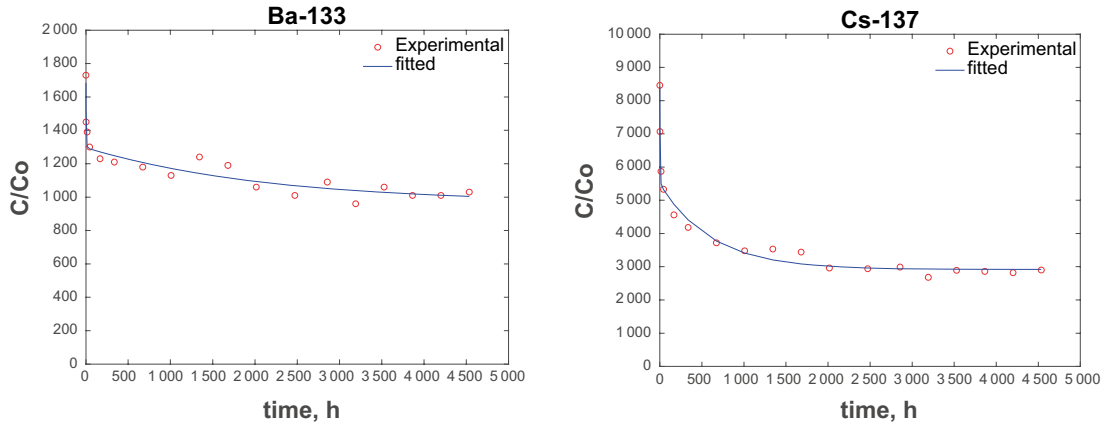

Figure A-3. *Activity of Ba-133 and Cs-137 in the reservoir as a function of time; experimental and fitted values.*

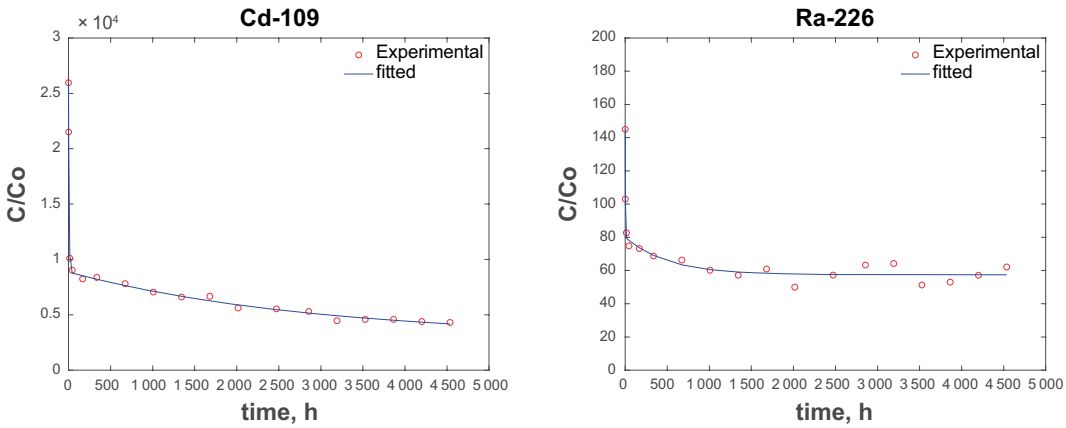

Figure A-4. *Activity of Cd-109 and Ra-226 in the reservoir as a function of time; experimental and fitted values.*

Appendix B

B1 Effective diffusivity and Capacity Factor for Cl-36

Table B-1. Effective diffusivity and capacity factor for Cl-36.

Core	De*E+13, m^2/s	Alpha	Square-sum*
A4	0.0095	0.0104	2.33E+00
A6	0.0150	0.0055	4.97E+00
A9	0.0072	0.0069	2.18E+00
A12	0.0063	0.0049	1.59E+00
A16	0.0085	0.0033	1.52E+00
A17	0.0107	0.0040	2.59E+00
D1	0.0377	0.0008	1.60E−01
D7	0.3626	0.0003	6.28E−02
D13	0.1694	0.0004	9.83E−02
D14	0.0038	0.0038	3.92E+00
D15	0.0044	0.0003	6.61E−02

* Square-sum = $\Sigma(Act_{exp} - Act_{calc})^2$

B2 Effective diffusivity and Capacity Factor for Na-22

Table B-2. Effective diffusivity and capacity factor for Na-22.

Core	De*E+13, m^2/s	Alpha	Square-sum*
A1	0.828	0.0253	5.05E+00
A4	0.118	0.0906	2.33E+01
A5	0.249	0.0112	1.96E+01
A6	0.403	0.0390	3.14E+02
A8	1.379	0.1922	6.77E+04
A9	0.129	0.0213	2.16E+01
A10	0.242	0.0106	5.99E+00
A11	0.350	0.0085	4.92E+00
A12	0.106	0.0163	2.76E+01
A15	0.346	0.0215	1.97E+02
A16	0.248	0.0162	6.07E+01
A17	0.463	0.0107	1.86E+01
D1	0.388	0.0475	4.92E+01
D5	0.173	0.0695	1.64E+02
D6	0.682	0.0250	5.72E+01
D7	1.465	0.0246	3.91E+01
D8	0.631	0.0294	8.36E+01
D12	1.178	0.0204	1.32E+01
D13	1.180	0.0238	7.52E+00
D14	1.513	0.0204	5.88E+01
D15	0.152	0.0199	3.74E+00
D16	0.456	0.0268	8.32E+00

* Square-sum = $\Sigma(Act_{exp} - Act_{calc})^2$

B3 Effective diffusivity and Capacity Factor for Ba-133

Table B-3. Effective diffusivity and capacity factor for Ba-133.

Core	De*E+13, m^2/s	Alpha	Square-sum*
A1	7.991	6.080	2.59E−01
A4	1.255	1.936	3.56E+00
A5	1.442	1.726	1.00E−10
A6	1.163	3.467	2.85E+02
A8	0.459	0.902	3.39E+01
A9	1.433	4.268	2.96E+01
A10	1.047	1.760	3.94E+00
A11	0.728	1.270	1.96E+01
A12	1.571	3.213	2.39E−01
A13	0.985	7.552	1.30E+01
A15	2.836	3.976	9.76E+01
A16	1.221	2.852	5.56E+01
A17	0.902	2.048	1.43E+00
D1	1.200	5.446	2.04E+00
D5	1.256	3.711	8.61E+00
D6	0.837	3.032	9.21E+00
D7	3.281	3.083	3.25E+02
D8	0.320	2.928	2.41E+03
D12	1.381	4.616	3.25E+02
D13	2.202	3.368	5.09E+01
D14	0.961	1.726	1.59E+02
D15	0.639	3.212	3.92E+01
D16	2.031	7.271	2.65E+01

* Square-sum = $\Sigma(Act_{exp} - Act_{calc})^2$

B4 Effective diffusivity and Capacity Factor for Cs-137

Table B-4. Effective diffusivity and capacity factor for Cs-137.

Core	De*E+13, m^2/s	Alpha	Square-sum*
A1	28.4	29.4	1.65E+01
A4	7.3	15.5	3.15E+02
A5	6.4	10.4	1.00E−10
A6	12.9	32.9	2.10E+06
A8	1.78	8.4	1.15E+03
A9	6.73	26.8	1.23E+02
A10	4.45	8.19	9.40E+02
A11	3.51	7.72	4.00E+02
A12	7.33	14.2	3.85E+02
A13	1.71	16.4	2.21E+01
A15	16.9	35.9	2.00E+03
A16	6.32	19.8	1.98E+03
A17	3.53	10.3	4.69E+01
D1	5.23	27.3	5.48E+01
D5	5.33	17.2	6.28E+02
D6	3.43	13.2	1.78E+03
D7	14.3	9.59	5.35E+04
D8	1.81	17.7	2.94E+05
D12	6.89	28	6.40E+04
D13	9	13.1	5.02E+04
D14	4.02	9.14	8.06E+04
D15	3.5	18.7	9.37E+03
D16	7.31	25.5	4.36E+03

* Square-sum = $\Sigma(Act_{exp} - Act_{calc})^2$

Arkitektkopia AB, Bromma, 2020

SKB is responsible for managing spent nuclear fuel and radioactive waste produced by the Swedish nuclear power plants such that man and the environment are protected in the near and distant future.

skb.se